iScience

CellPress
OPEN ACCESS

Article

A combination therapy of bortezomib, CXCR4 inhibitor, and checkpoint inhibitor is effective in cholangiocarcinoma *in vivo*

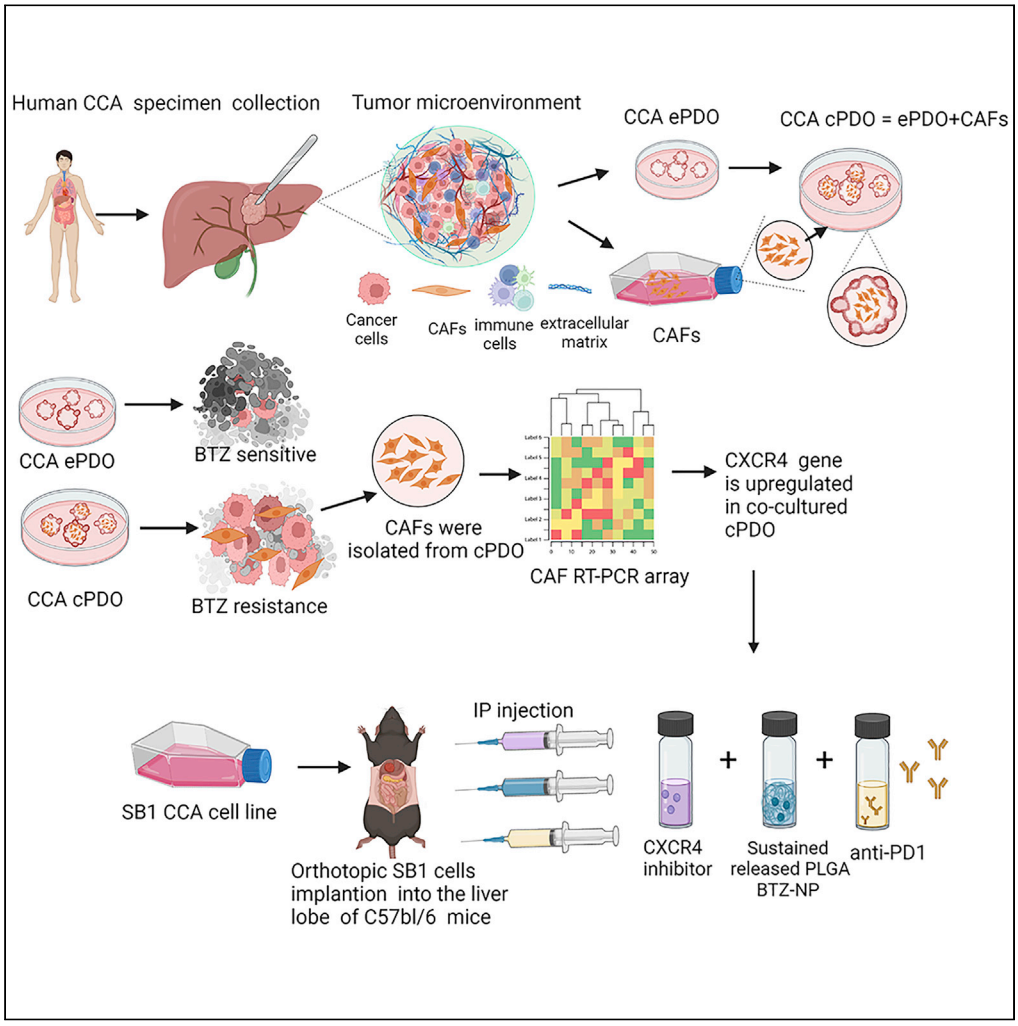

Ling Li, Yang Zhou, Yicheng Zhang, Haijie Hu, Hai-Quan Mao, Florin M. Selaru

fselaru1@jhmi.edu

Highlights

Stroma in CCA plays a fundamental role in tumor resistance to chemotherapy

Stroma in CCA plays a fundamental role in tumor immune surveillance

A combination inhibitors of cancer cells, stroma, and PD1 is effective in CCA

Li et al., iScience *26*, 106095
March 17, 2023 © 2023 The Authors.
https://doi.org/10.1016/j.isci.2023.106095

iScience

CellPress
OPEN ACCESS

Article

A combination therapy of bortezomib, CXCR4 inhibitor, and checkpoint inhibitor is effective in cholangiocarcinoma *in vivo*

Ling Li,[1] Yang Zhou,[2,3] Yicheng Zhang,[2,3] Haijie Hu,[1] Hai-Quan Mao,[2,3,4,5] and Florin M. Selaru[1,2,6,7,*]

SUMMARY

Cholangiocarcinoma (CCA) is a biliary tree malignancy with a dismal prognosis. Tumor microenvironment (TME), including cancer-associated fibroblasts (CAFs) has been shown to be involved in drug resistance. To model the interactions between cancer cells and the TME, we established CCA complex patient-derived organoids (cPDOs) to include epithelial PDO (ePDOs) and matched CAFs. While ePDOs were sensitive to bortezomib, we found the matched cPDOs were relatively resistant. Mechanistically, this resistance was correlated with over-expression of CXCR4 in the CAF component of cPDOs. In accord with the role of CXCR4 in the resistance to bortezomib, we found that a CXCR4 inhibitor can reverse the resistance to bortezomib *in vivo*. Furthermore, we found that the inhibition of CXCR4 allowed bortezomib to sensitize CCA to anti-PD1 treatment, with a significant reduction of tumor burden and long-term overall survival. This novel cancer/stroma/immune triple treatment holds great promise for the treatment of CCA.

INTRODUCTION

Cholangiocarcinoma (CCA) is a highly aggressive cancer emerging from the epithelium of the biliary tree. CCA accounts for 15% of all primary liver malignancies. CCA has a dismal prognosis with a 5-year overall survival (OS) rate of 10%, and a median OS of 24 months.[1,2] Surgical resection or liver transplantation are the only potentially curative approaches, but are feasible only in a minority of patients who are diagnosed early in their disease course.[3,4] Of note, even after resection with curative intent, approximately 70% of patients recur. Therefore, almost all patients with CCA require effective systemic treatment.[5] A number of recent studies have identified promising therapies for CCA. For example, durvalumab, an investigational anti-PD-L1 treatment is investigated in trials for CCA.[6] The recent years have also witnessed targeted therapies in combination with standard chemotherapy for CCA.[7] However current first-line therapy has a limited impact on outcomes.[5] CCAs are densely desmoplastic and their relative resistance to therapy is thought to be due, in large part, to activated cancer-associated fibroblasts (CAFs) that support cancer cells and render them resistant to chemotherapy as well as to immune therapies.[8]

Bortezomib (BTZ) is a proteasome inhibitor that is Food and Drug Administration (FDA) approved for multiple myeloma.[9] Bortezomib was reported to be effective *in vitro* in several cancers including CCA.[10–12] In a high-throughput drug screening on primary patient-derived organoids (PDO), we found that BTZ is highly effective against CCA cells *in vitro*.[13] These *in vitro* findings are in contrast to several human clinical trials which have not found BTZ effective in CCA, pancreatic cancer and hepatocellular carcinoma with desmoplastic features.[10–12] In corroborating these findings, we hypothesized that the clinical trial failures were not due to the cell-intrinsic potency of BTZ but rather due to the tumor microenvironment (TME) and CAFs that protect cancer cells from BTZ.

Immune checkpoint inhibitors (ICIs) hold promise in a variety of solid cancers. Patients treated with these agents oftentimes display increased survival and long-term remission. For these reasons, ICI has become a first-line drug for some of these malignancies.[14–17] In CCA, however, when used alone, ICIs have shown only a modest clinical benefit.[18] It was noted that CCAs display a relatively low infiltrate of T lymphocyte and immune positive modulating factors in the tumor mass.[19,20] Therefore, it was hypothesized that this relative ineffectiveness of ICI in CCA is at least in part due to the rich TME that CCAs display and which renders immune surveillance ineffective.

[1]Division of Gastroenterology and Hepatology, School of Medicine, Johns Hopkins University, Baltimore, MD 21205, USA

[2]Institute for NanoBioTechnology, Johns Hopkins University, Baltimore, MD 21205, USA

[3]Department of Materials Science and Engineering, Whiting School of Engineering, Johns Hopkins University, Baltimore, MD 21205, USA

[4]Department of Biomedical Engineering, Johns Hopkins University School of Medicine, Baltimore, MD 21205, USA

[5]Translational Tissue Engineering Center, Johns Hopkins University School of Medicine, Baltimore, MD 21205, USA

[6]Department of Oncology, Sidney Kimmel Cancer Center, School of Medicine, Johns Hopkins University, Baltimore, MD 21205, USA

[7]Lead contact

*Correspondence: fselaru1@jhmi.edu

https://doi.org/10.1016/j.isci.2023.106095

This is an open access article under the CC BY-NC-ND license (http://creativecommons.org/licenses/by-nc-nd/4.0/).

C-X-C chemokine receptor 4 (CXCR4) inhibitors were shown to decrease CAF activation and reverse the immunosuppression in the TME of several solid cancers, such as breast, pancreatic, hepatocellular cancer (HCC), glioblastoma, and others.[21–26] In addition, the combination of a CXCR4 inhibitor with a programmed cell death protein 1 (PD1) provided a significant benefit in preclinical animal models of cancer as well as in human clinical trials.[21–26] Of further importance, a high CXCR4 expression correlates with CCA progression and metastasis. In addition, the OS of patients with intrahepatic CCA correlates inversely with CXCR4 expression.[26] Last, activated CAF in the TME of CCA secretes stromal cell-derived factor-1 (SCF-1), which activates CXCR4 to induce CCA cell invasion via ERK1/2 and Akt.[24]

In this study, we hypothesized that combining a CXCR4 inhibitor with an anti-PD1 agent as well as BTZ can overcome the overall immunosuppressive TME. Firstly, using a human CCA PDO-derived subcutaneous PDX mouse model, we demonstrated that CXCR4 inhibition can decrease the activation of CAFs in CCAs and reverse BTZ resistance. In addition, using subcutaneous and orthotopic immunocompetent CCA mouse model, we report that a CXCR4 inhibitor increased the effectiveness of anti-PD1 in CCA sensitized with BTZ. The triple combination therapy resulted in a significant reduction in tumor size and long-term overall survival. This study provides the foundation of a novel effective therapy in CCA that can be applied in future clinical trials.

RESULTS

Establishment of a patient-derived epithelial organoid and matched patient-derived xenograft from a human cholangiocarcinoma specimen

As we reported previously, human CCA tissue obtained at surgery was utilized to establish an epithelial patient-derived organoid line (ePDO61).[13] The tumor utilized to establish this ePDO was a poorly differentiated intrahepatic cholangiocarcinoma with extensive necrosis. There was lymphovascular invasion. Two lymph nodes were positive for metastatic carcinoma. The ePDO61 was utilized to establish a matched patient-derived xenograft model (PDX61) by the implantation of ePDOs into NOD SCID-IL2R-γ chain-deficient (NSG) mice, as we have done previously.[27] Figures 1A–1C shows staining for cholangiocyte markers (CK7 and CK19), an epithelial marker (EPCAM) as well as a stem cell marker (LGR5). The similar staining pattern and intensity argue that ePDO61, as well as PDX61 represent suitable models of the primary CCA specimen. Hematoxylin and eosin (H&E) staining for these 3 matched tissues is shown in Figure 1D and further demonstrates a similar appearance.

Establishment of complex patient-derived organoids to include fibroblasts along with epithelial cancer cells

Human CCAs tend to be highly desmoplastic.[28] The dense stromal infiltrate is thought to participate in the survival of cancer cells through multiple mechanisms, including the inhibition of immune responses against the cancer.[28] To model some of these complex interactions between epithelial cancer cells and stromal cells (including fibroblasts) we aimed to develop cPDOs by 3-dimensional co-culturing of human tumor fibroblasts obtained from primary CCA resection specimens with epithelial cancer cells obtained from matched specimens. First, we isolated cancer-associated fibroblasts (CAFs) from the human CCA resection specimens and then verified their identity with a combination of CAF markers: alpha smooth muscle actin (α-SMA), Collagen-1, fibroblast specific protein-1 (FSP1), vimentin and fibroblast activation protein (FAP)[29–31] (Figure S1). Then, these CAFs were co-cultured with ePDOs established from the same tumor. Bright-field image and cell tracker live staining demonstrated the growth of a cystic epithelial organoid within a matrix of CAFs (Figures 2A and 2B). cPDO cultures were embedded in OCT on day 14 and slides were cut for immunostaining with the purpose of comparing against human tissue as well as PDX tissue. Figure 2C (panel 1) shows the self-organization of cPDO cultures with islands of CK7-stained CCA cells surrounded by collagen-1 secreted by CAFs in the co-culture. This appearance is strikingly similar to human CCA tissue, as well as CCA PDX *in vivo* (panels 2 and 3 in Figure 2C).

Drug testing in epithelial patient-derived organoids and matched complex patient-derived organoids

We previously reported a high throughput drug screening in ePDOs.[13] This previous effort identified BTZ as a highly effective drug with inhibitory concentration 50 (IC50) ranging from 1 nM to 30.37 nM across multiple liver cancer PDO lines. Here, we contrasted the IC50 of BTZ in three CCA ePDOs vs. matched cPDOs

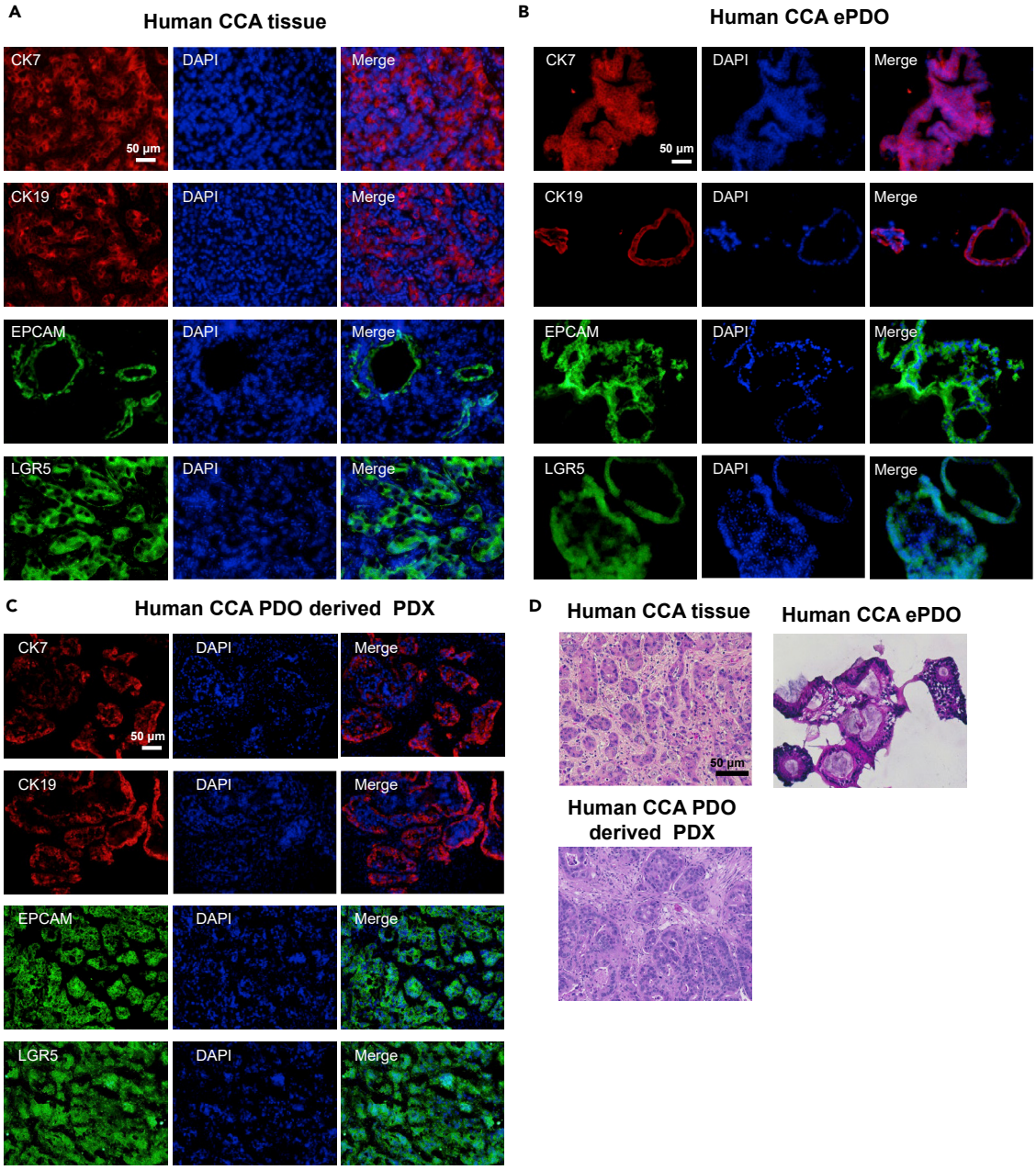

Figure 1. Primary human CCA is similar to a matched ePDO as well as PDO-derived PDX

(A–C) IF staining with antibodies anti-CK7 and -CK19, EPCAM, as well LGR5 is similar in primary CCA, matched ePDO and PDX. Scale bar - 50 µm

(D) H& E staining is similar in primary human CCA tissue and matched ePDO and PDX. Scale bar - 50 µm.

lines. We hypothesized that if CAFs participate in inducing resistance to BTZ, then we should see a higher value for IC50 in matched cPDOs vs. ePDOs. Indeed, as Figure 2D shows, a concentration of 10 nM of BTZ is sufficient to kill all cancer cells in the ePDO, while the same concentration is not sufficient in the matched cPDO. Further increases in the dose of BTZ in cPDO demonstrate that there are some live PDO cells even at a concentration of BTZ of 10 µM. The calculated IC50 of BTZ increased more than 100-fold in cPDOs vs. matched ePDOs in the three different CCA patient-derived PDOs (Figure 2E and Table 1). These results argue that CAFs in the cPDO are responsible, at least in part, for inducing resistance to BTZ. These results also argue that drug resistance mechanisms can be modeled *in vitro* by the addition of CAFs to ePDO cultures.

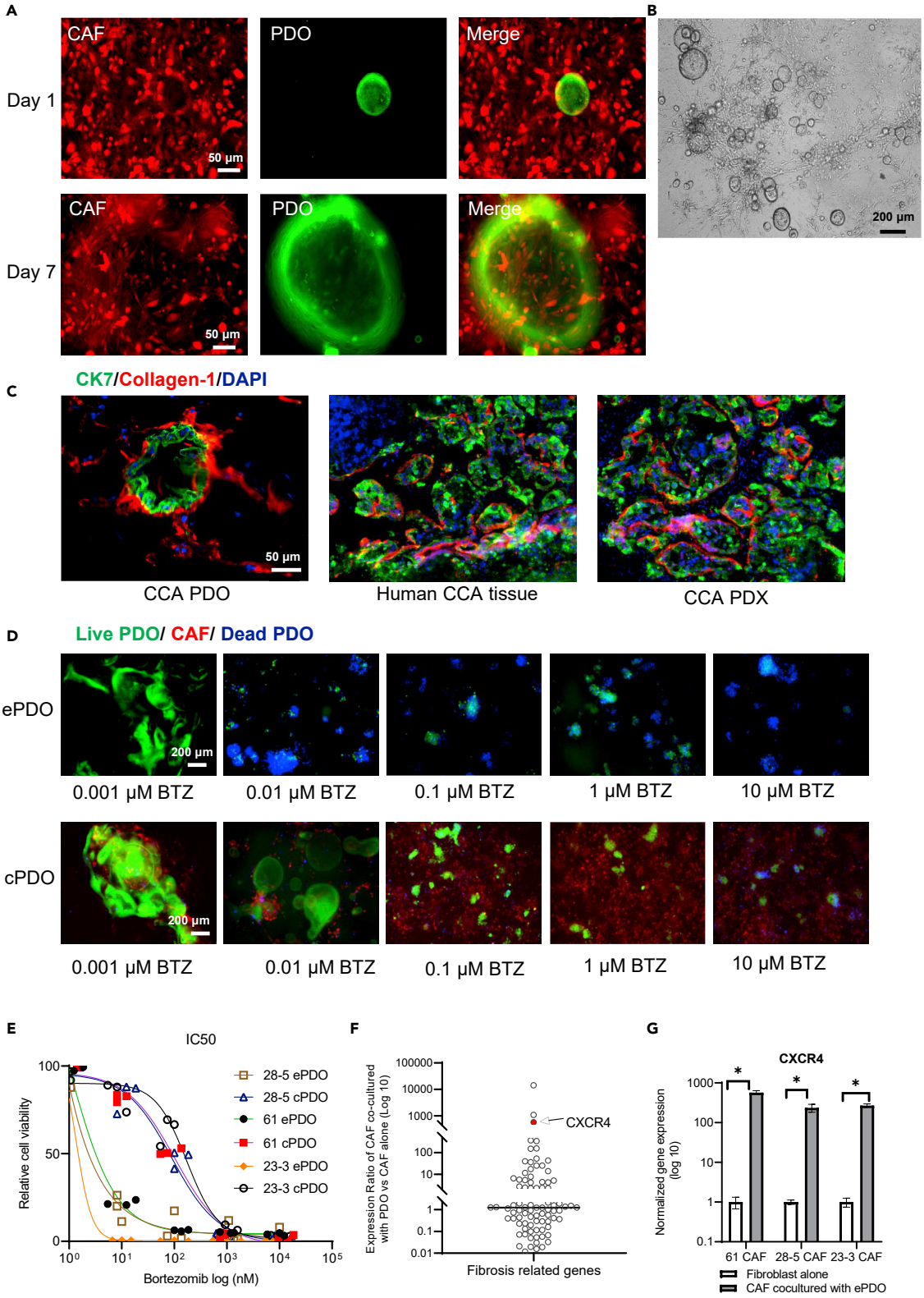

Figure 2. cPDOs are relatively resistant to BTZ when compared to matched ePDOs

(A) 3D co-cultures of CAFs (stained with cell tracker red) and CCA cells (stained with cell tracker green) were followed for 14 days. Live images are shown on Day 1 and Day 7. Scale bar - 50 μm.

Figure 2. *Continued*

(B) Bright-field image shows cystic-shaped epithelial organoids surrounded by spindle-shaped CAFs in the 3D culture on day 14.

(C) The self-organization of cPDOs is strikingly similar to matched human CCA tissue as well as matched PDX tissue. CK7 stains CCA cells in the figure. Collagen produced by CAFs is stained in the figure as well. Scale bar - 50 μm.

(D) Increasing concentrations of BTZ from 0.001 to 10 μM have a differential effect on ePDO and matched cPDO cultures at 96 h. Green – Live CCA PDO cells, Blue - Dead CCA PDO cells, Red - CAFs. Scale bar - 200 μm.

(E) IC50 curves are calculated and displayed for three ePDO vs. matched cPDO.

(F) qRT-PCR array shows differentially expressed genes in CAFs co-cultured with ePDO vs. fibroblasts grown without cancer. The arrow indicates CXCR4, which was found to be upregulated approximately 500-fold.

(G) qRT-PCR shows that CXCR4 is upregulated in CAFs co-cultured with ePOD from three patients with CCA (61 CAF - 570-fold; 28-5 CAF- 200-fold; and 23-3CAF - 250-fold respectively compared with fibroblasts alone), n = 3, paired two-sided Student's *t* test Data were present as Mean ± SEM, *$p < 0.05$.

Evaluation of fibroblast gene expression in complex patient-derived organoids

To further explore the mechanism of relative BTZ resistance in cPDO vs. matched ePDO, we contrasted gene expression in CAFs isolated from the cPDO61 vs. the same fibroblasts grown without cancer cells. A qRT-PCR array including a panel of 80 human fibrosis-related genes was performed and CXCR4 was found to be upregulated 500-fold in CAFs vs. the same fibroblasts grown without cancer cells (Figure 2F). To confirm the upregulation of CXCR4 in co-cultured CAF, RT-PCR was applied to measure CXCR4 gene expression in CAFs isolated from 3 different CCA patient-derived cPDOs vs. the same fibroblasts grown without cancer cells. As shown in Figure 2G, CXCR4 was upregulated 250- to 500-fold. Although there were other genes that were upregulated in CAFs, we chose CXCR4 for further studies because of its known role in CCA in previous studies[24,26,32] and the fact that there are FDA-approved small molecule inhibitors of CXCR4.

In vivo dual treatment with bortezomib-NP and a CXCR4 inhibitor

NSG mice carrying subcutaneous PDX61 tumors were treated with BTZ or combination of BTZ and plerixafor, an inhibitor of CXCR4. BTZ was given intra-tumorally, in a nanoparticle formulation that provides a sustained release for 5 days[33] (Figures S2 and 3A - panel 1). As shown in Figures 3B and 3C, adding plerixafor increased the ability of BTZ to suppress CCA growth *in vivo*. H&E staining is shown in Figure 3D demonstrating less tumor cells in the combination treatment.

The impact of CXCR4 inhibition on stroma

Molecular studies on the PDX61 model demonstrated that there are more cleaved caspase 3 positive apoptotic cells (Figures 4A and 4C), less proliferative Ki67 positive as well as less CK19-positive cancer cells in the combination treatment arm vs. BTZ group (Figures 4B, 4E, and 4F). In addition, we found that the combination of BTZ with the CXCR4 inhibitor therapy decreased the α-SMA positive CAF cells in the tumor mass (Figures 4B and 4D). There results argue that the CXCR4 inhibitor can reduce the CAFs in CCA. Furthermore, we conclude that the relative resistance to BTZ in cPDO is, at least in part, due to CAFs and that their impact can be diminished by treatment with a CXCR4 inhibitor.

In vivo combined treatment with bortezomib-NP, a CXCR4 inhibitor, and a checkpoint inhibitor

In addition to the effects on stroma, CXCR4 was noted to enhance the effects of immune checkpoint inhibitors in several solid cancers.[21,23,25,34,35] Based on these studies, we formulated the hypothesis that the inhibition of CXCR4 would allow a checkpoint inhibitor to more successfully stimulate the activity of immune cells that, by extension, would be more effective against cancer cells treated with BTZ. To test this hypothesis, we implemented the treatment regimens shown in Figure 4A (panels 2 and 3), in an immunocompetent

Table 1. IC50 of BTZ in cPDOs vs. matched ePDOs in the three different CCA patient-derived PDOs

	IC50 (nM)	
PDOs	ePDO	cPDO
23–3	171.9	1.35
28–5	89	0.1
61	103.9	1.027

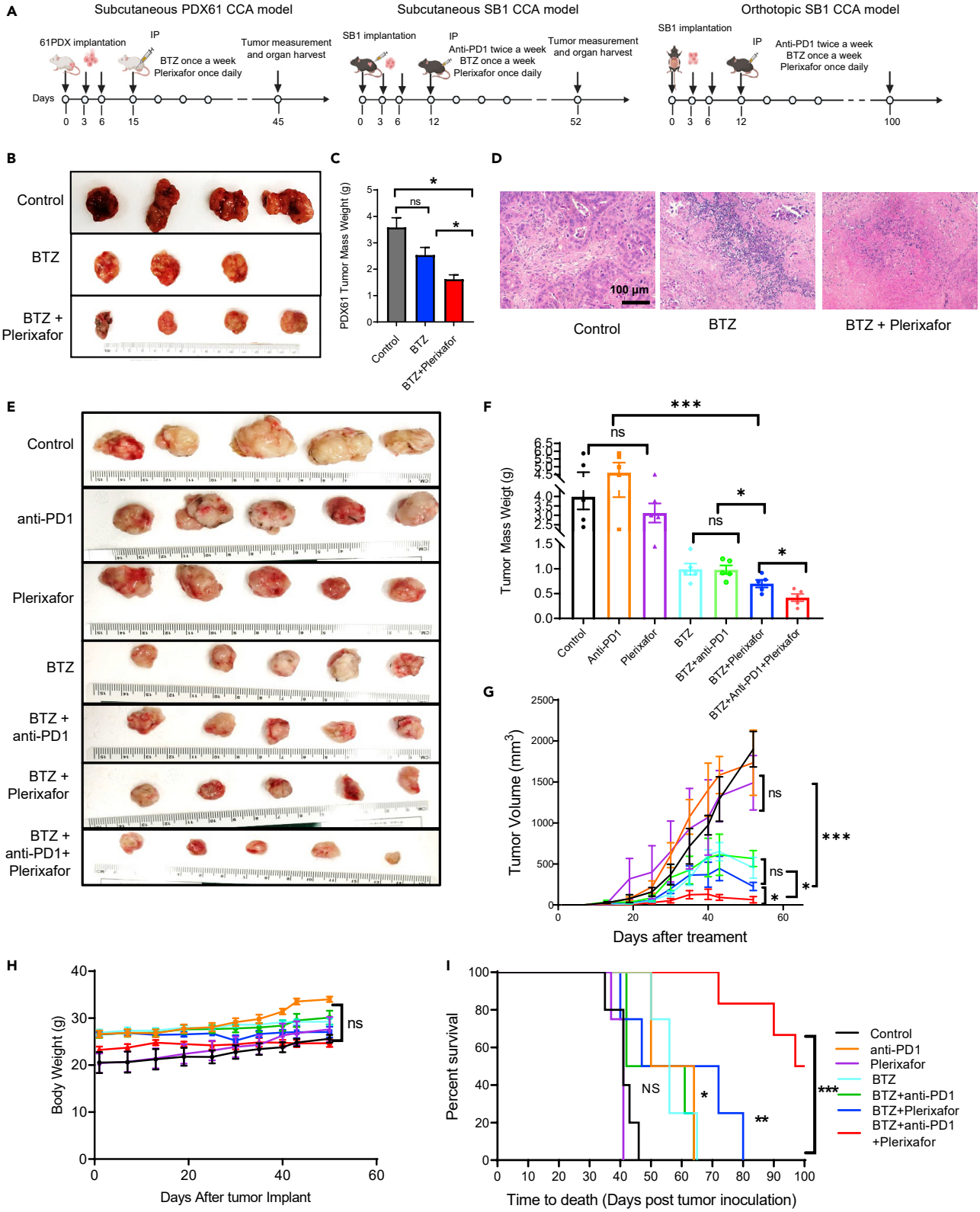
A
Subcutaneous PDX61 CCA model
61PDX implantation
IP
BTZ once a week
Plerixafor once daily
Tumor measurement and organ harvest
Days
0 3 6 15 45
Subcutaneous SB1 CCA model
SB1 implantation
IP
Anti-PD1 twice a week
BTZ once a week
Plerixafor once daily
Tumor measurement and organ harvest
0 3 6 12 52
Orthotopic SB1 CCA model
SB1 implantation
IP
Anti-PD1 twice a week
BTZ once a week
Plerixafor once daily
0 3 6 12 100
B
Control
BTZ
BTZ + Plerixafor
C
PDX61 Tumor Mass Weight (g)
ns
*
*
Control
BTZ
BTZ+Plerixafor
D
100 μm
Control
BTZ
BTZ + Plerixafor
E
Control
anti-PD1
Plerixafor
BTZ
BTZ + anti-PD1
BTZ + Plerixafor
BTZ + anti-PD1+ Plerixafor
F
Tumor Mass Weigt (g)
***
ns
*
ns
*
Control
Anti-PD1
Plerixafor
BTZ
BTZ+anti-PD1
BTZ+Plerixafor
BTZ+Anti-PD1+Plerixafor
G
Tumor Volume (mm3)
ns
ns
***
*
*
Days after treament
H
Body Weight (g)
ns
Days After tumor Implant
I
Percent survival
NS
*
**
***
Control
anti-PD1
Plerixafor
BTZ
BTZ+anti-PD1
BTZ+Plerixafor
BTZ+anti-PD1 +Plerixafor
Time to death (Days post tumor inoculation)

Figure 3. BTZ, plerixafor, and anti-PD1 treatments are effective *in vivo* in models of CCA

(A) Schematic of drug administration for BTZ, plerixafor and anti-PD1 in subcutaneous and orthotopic CCA models.

(B) Gross images of tumors from each of the 3 treatment arms are shown in the 61PDX mouse model.

(C) A bar graph depicts the statistically significant decrease of tumor mass in the combined vs. the BTZ alone arm in the 61PDX mouse model. $p < 0.05$, $n = 3$-4.

(D) H& E staining of CCA PDX from each of the 3 treatment arms are shown in the 61PDX mouse model. Scale bar - 100 μm.

(E) Gross images of tumors from tumor-bearing mice treated with different combination treatments in SC SB1 CCA mouse model.

(F) A plot of tumor weights at the end of treatment in the SC SB1 mouse model.

(G) A plot of tumor sizes in the SB1 CCA mouse model. Tumor volumes were measured twice a week after the inoculation until endpoint.

(H) A plot of body weights for all treatment groups in the SC SB1 CCA mouse model, n = 5, unpaired two-sided Student's *t* test Data were present as Mean ± SEM, *<0.05, **<0.01 *** < 0.001. NS - no statistical significance.

(I) Survival curve of mice bearing orthotopic SB1 CCA, n = 5. *<0.05, **<0.01 *** < 0.001. NS - no statistical significance. Survival significance was determined via log-rank test.

mouse CCA model, as previously described.[36] We implemented 2 variants of this immunocompetent CCA model—a subcutaneous model (for ease of serial measurements of subcutaneous tumors) and an orthotopic model (for better modeling of cancer for survival studies). As shown in Figures 4E–4G, anti-PD1 treatment alone did not have an effect on tumors, mirroring clinical experience with anti-PD1 in patients with CCA. Similarly, CXCR4 inhibition alone did not impact tumors in a significant manner. Treatment with BTZ alone decreased the weight (Figure 4F) and size (Figure 4G) of tumors, as expected. While the combination of BTZ and anti-PD1 did not appear to be more effective than BTZ alone, the combination of BTZ and CXCR4 inhibition appeared more effective at controlling tumor size than BTZ alone. Finally, the combination of BTZ, CXCR4 inhibitor, and PD1 inhibitor was the most effective at controlling tumor weight and size. In regards to safety, none of the treatments had a significant negative effect on animals, as demonstrated by similar weight in each of the arms (Figure 4H). Since orthotopic models are felt to more closely model human disease, we chose to use such a model for survival studies. As shown in Figure 4I, BTZ with CXCR4 combination improved the overall survival in this SB1 orthotropic CCA model, bringing further proof that CXCR4 inhibition allows uninhibited tumor killing prompted by BTZ. However, as shown, triple therapy was even more efficacious in terms of extending survival, likely secondary to immune activation prompted by anti-PD1 treatment.

The impact of CXCR4 inhibition on fibrosis and immunity

To explore how CXCR4 inhibition facilitates enhanced anticancer activity, we performed real-time PCR on RNA extracted from bulk SB1 CCA tumors treated with each drug combination. We selected genes relevant to fibrosis, TME, as well as immune responses based on published work.[34] As shown in Figure 5A, CXCR4 inhibition alone significantly inhibited several fibrosis-related genes. In addition, CXCR4 inhibition alone also significantly upregulated Interferon gamma (Ifng), Granzyme A (Gzma), and Granzyme B (Gzmb), which are critical anti-tumor immunity genes, while inhibiting immune-suppressive genes (Figure 5B). BTZ treatment alone upregulated Ifng and Gzma but left the rest of the genes mostly unaffected. Most importantly, the triple therapy significantly increased T cell activation markers (Ifng, Gzma) (Figure 5C), while decreasing several immune-suppressive and checkpoint markers (Fasl, IL10, Tgfb1, Tim3, and PDCD4) (Figure 5D). These results suggested the triple therapy induced an immunostimulatory TME.

The impact on immune cells distribution as well as cytokines of combined therapy with bortezomib-NP, CXCR4 inhibition, and immune checkpoint inhibition

To further investigate the mechanism of action of triple therapy, we examined the immune cell infiltration and distribution in tumor mass via immune fluorescence staining, as shown in Figures 6A, 6D, and 6E, we found no increase in the numbers of $CD8^+$ T cells infiltrating the tumor mass (CK19 positive) in BTZ treatment alone. In contrast, there was a slight increase of CD8 cells in the BTZ + CXCR4 group as well as in the BTZ + anti-PD1 group. However, the triple therapy resulted in a massive cytotoxic T lymphocyte infiltration into the tumor mass and killing of CK19-positive CCA cells. Figures 6B, 6C, and 6F demonstrated that there were less Ki67-positive proliferative cells as well as more apoptotic cleaved caspase 3 positive cells in the triple therapy arm, corresponding with more $CD45^+$, $CD8^+$ immune cell infiltration.

To obtain further clarity in regards to immune cell infiltration of tumors for each treatment arm, we performed flow cytometry on single cell suspensions obtained from tumors from each treatment arm, similar to previous studies[25,34] (Figures 7A–7H). $CD45^+$ $CD3^+$ T lymphocytes and $CD4^+$ T helper cells are increased by plerixafor, plerixafor + BTZ as well as by the triple therapy (Figures 7A–7C). However, $CD8^+$ cytotoxic T

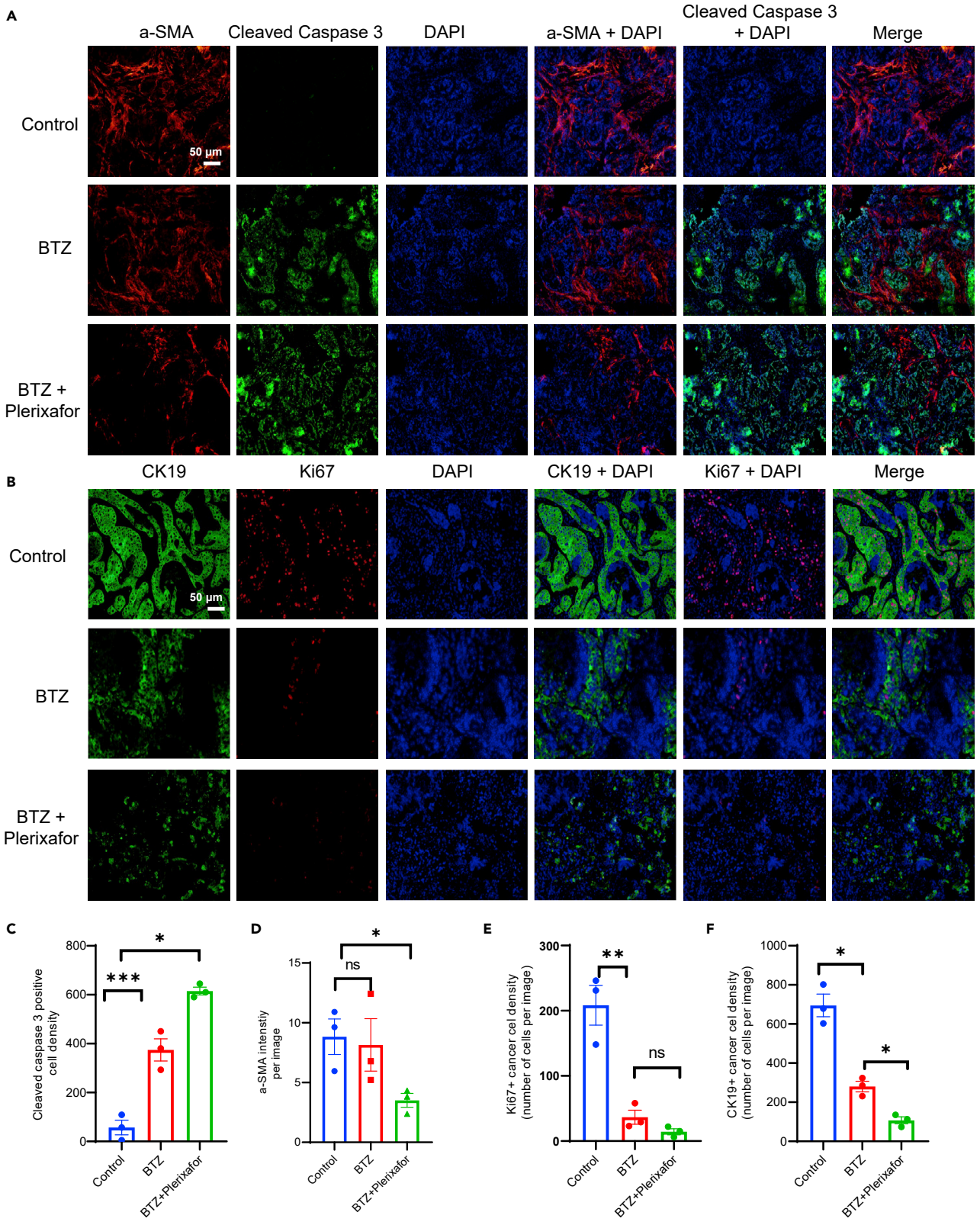
A
a-SMA
Cleaved Caspase 3
DAPI
a-SMA + DAPI
Cleaved Caspase 3 + DAPI
Merge
Control
BTZ
BTZ + Plerixafor
50 μm
B
CK19
Ki67
DAPI
CK19 + DAPI
Ki67 + DAPI
Merge
Control
BTZ
BTZ + Plerixafor
50 μm
C
Cleaved caspase 3 positive cell density
800
600
400
200
0
***
*
Control
BTZ
BTZ+Plerixafor
D
a-SMA intenstiy per image
15
10
5
0
ns
*
Control
BTZ
BTZ+Plerixafor
E
Ki67+ cancer cel density (number of cells per image)
300
200
100
0
**
ns
Control
BTZ
BTZ+Plerixafor
F
CK19+ cancer cel density (number of cells per image)
1000
800
600
400
200
0
*
*
Control
BTZ
BTZ+Plerixafor

Figure 4. BTZ combined with plerixafor inhibited the proliferation of cancer cells and activation of CAFs

(A) IF staining showed that BTZ combined with plerixafor induced cancer cell apoptosis (cleaved caspase 3 positive) and reduced desmoplasia (α-SMA positive). Scale bar - 50 μm.

(B) IF staining showed that BTZ combined with plerixafor decreased the proportion of Ki67-positive proliferative cells as well as CK19-positive live tumor cells. Scale bar - 50 μm.

(C) Quantification of cleaved caspase 3 positive cells in three treatment groups.

(D) Quantification of α-SMA positive cells in three treatment groups.

(E) Quantification of Ki67-positive cells in three treatment groups.

(F) Quantification of CK19-positive cells in three treatment groups. n = 3, unpaired two-sided Student's *t* test Data were present as Mean ± SEM, *<0.05, **<0.01 *** < 0.001. NS - no statistical significance.

lymphocyte are only increased by plerixafor + BTZ treatment and even more significantly by the triple therapy (Figure 7D). In addition, triple combination significantly decreased the amount of $CD45^+$ $F4/80^+$ tumor-associated macrophages in the tumor mass compared with all rest groups (Figures 7E and 7F). Furthermore, there were no changes in Cr1+ MSDCs as well as $CD11b^+$ DC cells in triple treatment groups compared with control (Figures 7G and 7H). These FACS results indicated that the triple combination therapy turned the "cold" immunosuppressive CCA MET into a "hot" immune-activated environment.[25,34]

To evaluate $CD8^+$ cytotoxic T lymphocytes activation, cytokines of T lymphocyte activation markers were determined with ELISA on bulk tumor extracts.[25,34] As shown in Figures 7I–7K, the triple therapy significantly increased T lymphocytes activation related cytokines IFN-γ, IL-2, and TNF-α. The level was increased by 2- to 4-fold for the triple therapy, while BTZ + CXCR4 inhibitor therapy increased IFN-γ, IL-2, and TNF-α

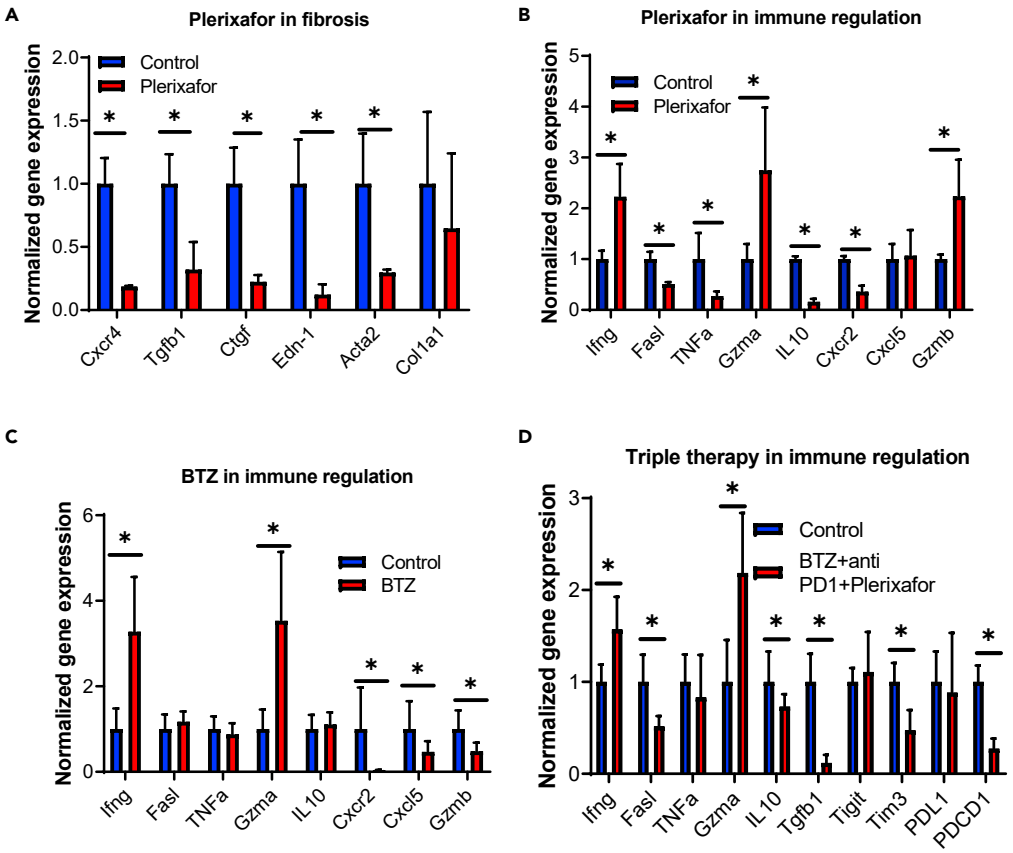

Figure 5. Combined therapy has a significant impact on immune cell regulation

(A) Plerixafor inhibits several fibrosis genes.

(B) Plerixafor affects immune response-related genes.

(C) BTZ alone has a minimal impact on immune response-related genes.

(D) Triple therapy has a significant impact on immune response-related gene expression. Unpaired two-sided Student's *t* test. Data were present as Mean ± SEM (n ≥ 4), * <0.05.

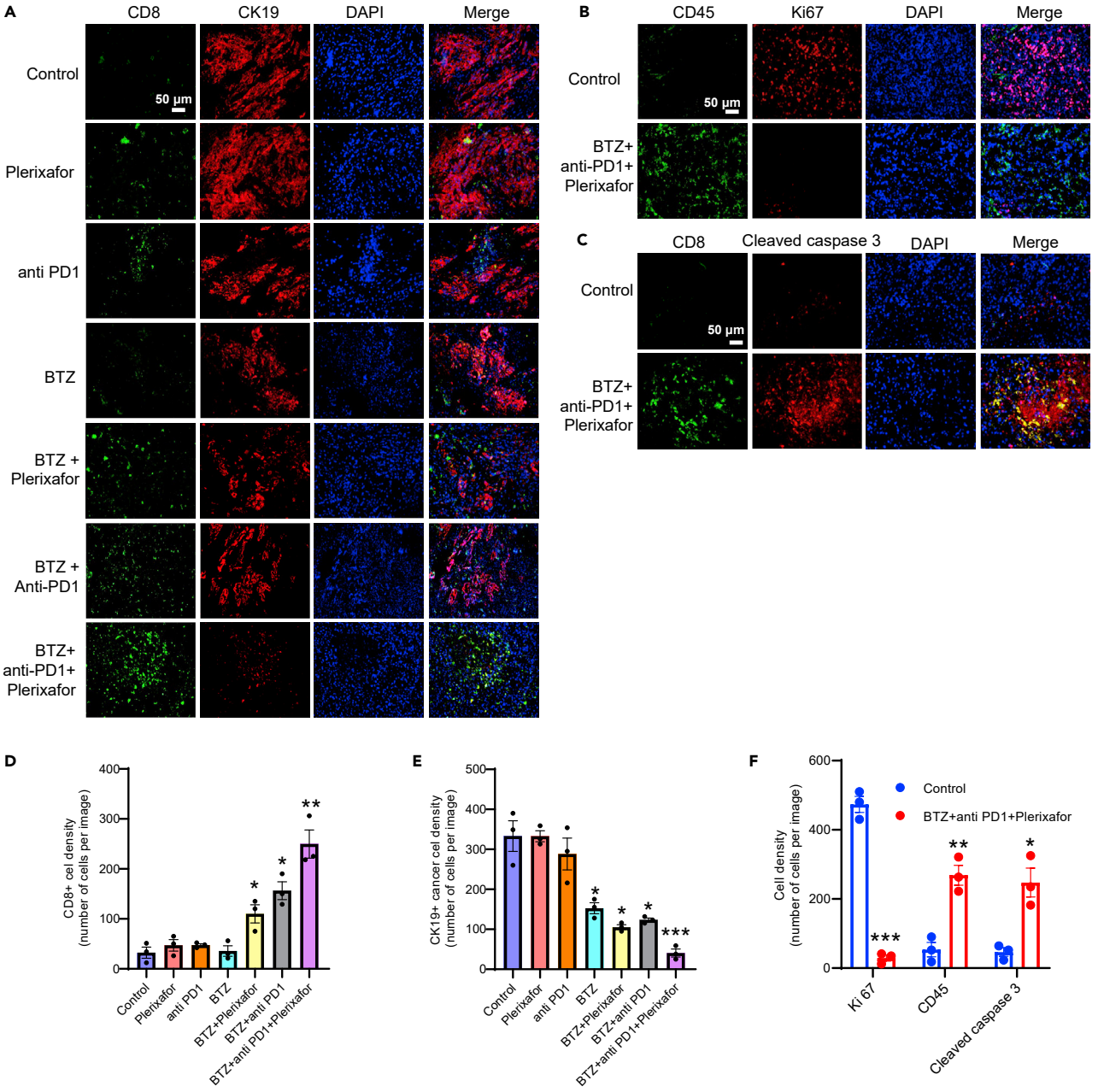

Figure 6. Triple therapy induces the infiltration of T lymphocytes into tumor mass

(A) Orthotopic SB1 CCA IF staining showed fewer CK19-positive tumor cells, but more tumor-infiltrated $CD8^+$ cytotoxic T cells in the triple therapy group.

(B and C) Triple therapy results in infiltration with $CD45^+$ and $CD8^+$ cells, less staining with Ki67 indicating less proliferation, and more staining with cleaved caspase 3, indicating increased apoptosis. Scale bar - 50 µm.

(D) Quantification of $CD8^+$ cells in all treatment groups.

(E) Quantification of CK19-positive cells in all treatment groups.

(F) Quantification of Ki67-positive cells, $CD45^+$ cells and cleaved caspase 3 positive cells in three combination treatment as well as the control group. n = 3, unpaired two-sided Student's *t* test Data were present as Mean ± SEM, *<0.05, **<0.01 *** < 0.001.

levels by 1.4-2.4-fold compared to control. The rest of the treatments only slightly increased the TNF-α levels vs. control while there is no significant changes in IFN-γ and IL-2. Therefore, triple combination therapy indicated the most positive activation of TME to facilitate the $CD8^+$ cytotoxic T lymphocytes activation toward killing tumor cells.

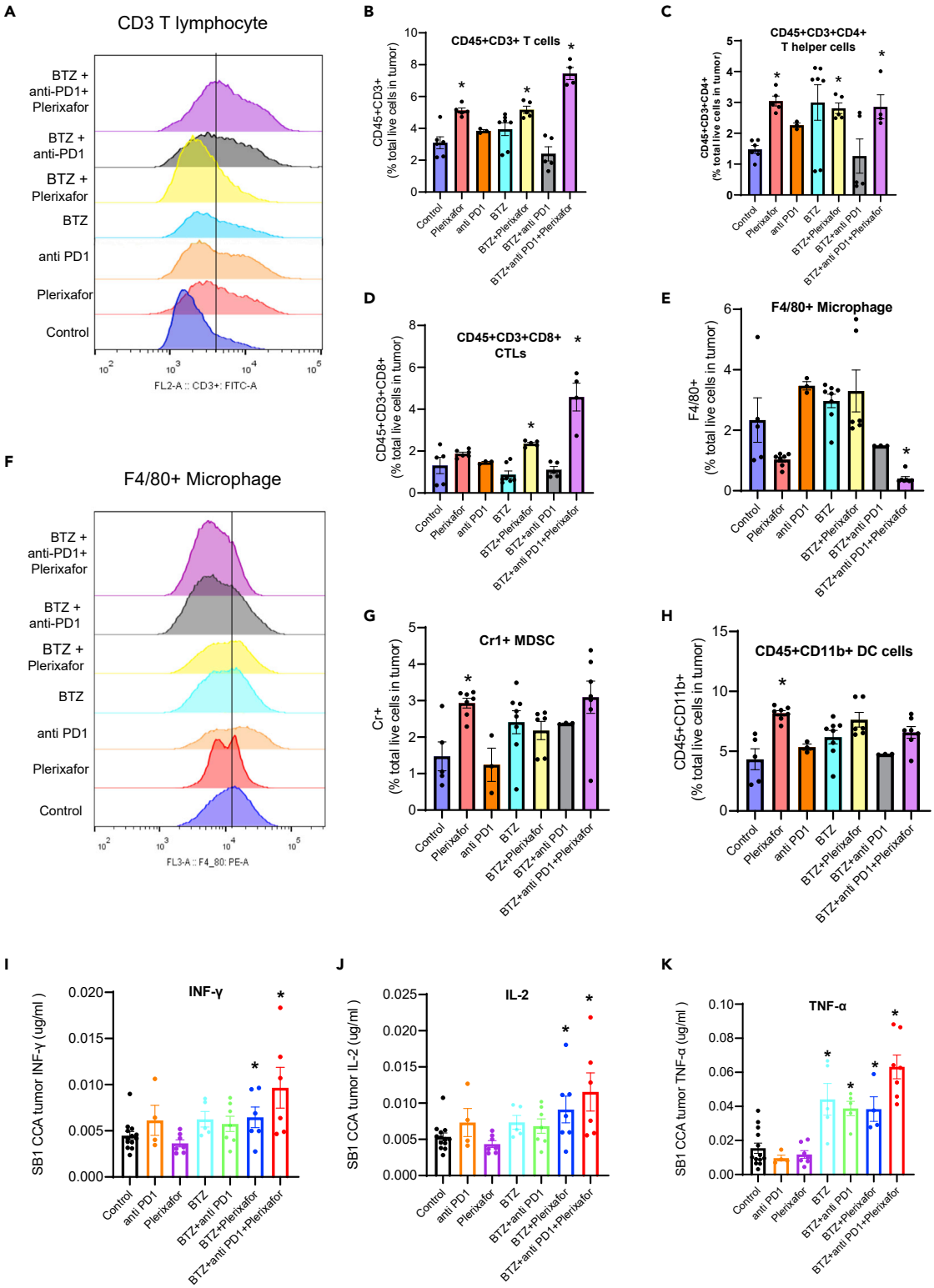
A
CD3 T lymphocyte
BTZ + anti-PD1+ Plerixafor
BTZ + anti-PD1
BTZ + Plerixafor
BTZ
anti PD1
Plerixafor
Control
FL2-A :: CD3+: FITC-A
B
CD45+CD3+ T cells
CD45+CD3+ (% total live cells in tumor)
C
CD45+CD3+CD4+ T helper cells
CD45+CD3+CD4+ (% total live cells in tumor)
D
CD45+CD3+CD8+ CTLs
CD45+CD3+CD8+ (% total live cells in tumor)
E
F4/80+ Microphage
F4/80+ (% total live cells in tumor)
F
F4/80+ Microphage
FL3-A :: F4_80: PE-A
G
Cr1+ MDSC
Cr+ (% total live cells in tumor)
H
CD45+CD11b+ DC cells
CD45+CD11b+ (% total live cells in tumor)
I
INF-γ
SB1 CCA tumor INF-γ (ug/ml)
J
IL-2
SB1 CCA tumor IL-2 (ug/ml)
K
TNF-α
SB1 CCA tumor TNF-α (ug/ml)
Control
anti PD1
Plerixafor
BTZ
BTZ+anti PD1
BTZ+Plerixafor
BTZ+anti PD1+Plerixafor

Figure 7. Flow cytometry analysis showed that triple therapy transforms a cold immunosuppressive environment into a hot immune activation environment; Cytokine analysis via MSD multi-spot assay showed T lymphocyte activation-related cytokines are upregulated in triple therapy compared with control

(A–D) Flow cytometry data showed there are much more 7AAD$^-$ CD45$^+$ CD3$^+$ T lymphocytes, 7AAD$^-$ CD45$^+$ CD3$^+$ CD8$^+$ CTLs as well as 7AAD$^-$ CD45$^+$ CD3$^+$ CD4$^+$ T helper cells in the triple therapy group.

(E and F) Flow cytometry data showed that there are less F4/80$^+$ macrophages in the triple treatment group, however, (G-H) There is no significant difference with 7AAD$^-$ CD45$^+$ Cr1$^+$ MDSC and 7AAD$^-$ CD45$^+$ CD11b$^+$ DC cell in triple treatment compared with control. Unpaired two-sided Student's *t* test. Data were present as Mean ± SEM (n ≥ 4), * <0.05.

(I-K) Cytokine analysis of IFN-γ, IL-2. and TNF-α. Unpaired two-sided Student's *t* test. Data were present as Mean ± SEM (n ≥ 4), * <0.05.

DISCUSSION

CCA is a highly desmoplastic tumor, with a dense fibrotic and immune infiltrate.[37] Accumulating evidence indicates that TME renders CCAs resistant to treatment, by either direct drug metabolization or through decreasing immune surveillance.[37] While immune checkpoint inhibitors (ICI) represent a promising therapeutic approach in many malignancies, in CCA, ICI alone confers minimal benefit.[18,38] A rationally designed combination therapy that modulates the TME to allow uninhibited drug treatment of cancer cells, as well as increased immune surveillance, is needed to impact outcomes for patients with CCA. We hypothesized that a combination of (1) a small molecule effective in CCA in a cell-intrinsic fashion with (2) a small molecule that inhibits TME and (3) an ICI molecule to dis-inhibit immune surveillance, will have a significant effect in CCA. Here we report that the novel combination of a proteasome inhibitor, a CXCR4 inhibitor, and a PD1 inhibitor significantly impact CCA growth and extend survival in relevant *in vivo* models. The data presented herein lays the foundation for human clinical trials that have the potential of changing the treatment paradigm in this lethal cancer.

Although TME is known to play major roles in CCA treatment, the relative paucity of animal models to accurately portray the interplay between stroma and epithelial cancer cells has been a major limitation to drug discovery efforts. Here, we report, for the first time in CCA, an *in vitro* model of human CAF-cancer interactions that is able to model stroma-cancer interactions *in vivo*. For example, in our system, we found that CAFs increase IC50 for BTZ by 11-fold, in accord with previous data that show BTZ is active against CCA in culture systems *in vitro*, but relatively resistant *in vivo* where CAFs are present. In addition, we show how this co-culture system allowed the identification of CXCR4 as a key player in CCA.

The derivation of a PDO-based PDX model is also of importance. The establishment of PDO and PDX models is difficult for liver cancers.[39] The ability to first establish PDO lines, and then implant these cancer PDO lines into immunosuppressed mice to derive PDX models is of major importance to further *in vivo* studies. Here we show that this PDX model showed similar desmoplastic features as the original CCA tumor. In addition, we were able to utilize this PDX model to evaluate if our hypothesis that CXCR4 inhibition can indeed render CCA sensitive to BTZ *in vivo* is correct. Indeed, we have shown that by adding CXCR4 inhibition to BTZ, the CCA tumor growth was inhibited, and the overall survival was extended. In addition, we were able to utilize this model to show that CXCR4 inhibition decreases α-SMA expression which offers a mechanistic understanding of how the treatment works.

Recent studies have shown that CXCR4 along with its ligand CXCL12 are involved in the negative modulation of the immune TME in breast, pancreatic cancer, and HCC.[21,23,25,34,35] In addition, it was shown that blocking the CXCR4-CXCL12 pathway results in enhanced activity of immune cells such as T lymphocytes.[21,23,25,34,35] By extension, it was shown that CXCR4 inhibitors facilitated tumor sensitivity to ICI therapy. In addition, CXCR4 inhibition was previously shown to decrease the ability of the stroma to counteract the effects of chemotherapy.[21,23,25,34,35] In this study, we showed that inhibiting CXCR4 results in the augmentation of the effects of BTZ. In addition, we also showed that in CCA, a highly desmoplastic cancer, the triple therapy with BTZ, CXCR4 inhibition, and PD1 inhibition showed the greatest controlling of tumor growth as well as the best overall survival *in vivo*. Using flow cytometry as well as immune fluorescence staining, infiltration of activation of the immune cell population in treated CCA tissue was analyzed. The results showed that anti-PD1 alone was ineffective for promote the effect of immune cells to infiltrate and activate in the tumor, which was in line with 2 recent reports in CCA,[40,41] CXCR4 inhibitor alone showed an increased amount of CD3$^+$ and CD4$^+$ T lymphocyte, but showed no effect on tumor growth and overall survival, CXCR4 inhibitor combined with BTZ promote CD3$^+$ and CD4$^+$ as well as CD8 T lymphocyte with moderate inhibition of tumor growth and survival extension. Of note, triple combination showed the maximal increase of CD3$^+$, CD4$^+$ as well CD8$^+$ T lymphocytes and decreased F4/80$^+$ tumor-associated macrophages. This immune cell population changes indicated that triple therapy overcomes the immune-suppressive TME and promotes the best synergistic therapy effect.

In summary, the triple therapy of BTZ, CXCR4 inhibition, and PD1 inhibition showed the best inhibition of tumor growth as well as the longest overall survival in CCA. This study provides an encouraging preclinical foundation that requires further validation for possible application in human clinical trials. Further questions need to be answered, such as the duration of the BTZ sustained release, as well as the mode of delivery to patients. A percutaneous, ultrasound-guided, needle injection appears possible, however, such an approach needs to be investigated. Both CXCR4 inhibition, as well as immune checkpoint inhibitor options do exist in the clinic, however, a sustained release formulation of BTZ that is injected intra-tumorally would have to be cleared by the FDA prior to utilization in the clinic.

Limitations of the study

The findings of this study need to be validated through further preclinical work, as well as human trials. The impact of stroma on cancer drug metabolism and ultimately, the response to chemotherapy, requires careful validation prior to clinical translation.

STAR★METHODS

Detailed methods are provided in the online version of this paper and include the following:

- KEY RESOURCES TABLE
- RESOURCE AVAILABILITY
  - Lead contact
  - Materials availability
  - Data and code availability
- EXPERIMENTAL MODEL AND SUBJECT DETAILS
- METHOD DETAILS
  - CCA patients and samples
  - PDO and cell line culture
  - Drug testing in complex CCA PDOs
  - Sustained release BTZ-loaded nanoparticle formulation
  - Animal studies
  - Flow cytometry (FACS) analysis
  - Gene expression analysis
  - Electrochemiluminescence (ECL) assay
  - Histology and immunofluorescence (IF) staining
- QUANTIFICATION AND STATISTICAL ANALYSIS

SUPPLEMENTAL INFORMATION

Supplemental information can be found online at https://doi.org/10.1016/j.isci.2023.106095.

ACKNOWLEDGMENTS

This study was supported by Maryland Innovation Initiative (MII) Grants #0118-008_2 and #0320-008 to Florin M. Selaru and Hai-Quan Mao.

AUTHOR CONTRIBUTIONS

Study concept and design (FMS, LL, HQM), acquisition of data (LL, YZ, YZ, HH), analysis and interpretation of data (LL, YZ, HQM, FSM), drafting of the article (LL, YZ), critical revision of the article (HQM, FMS), statistical analysis (LL, YZ, YZ).

DECLARATION OF INTERESTS

The authors have declared that no conflict of interest exists.

Received: August 2, 2022
Revised: January 4, 2023
Accepted: January 26, 2023
Published: January 31, 2023

REFERENCES

1. Banales, J.M., Marin, J.J.G., Lamarca, A., Rodrigues, P.M., Khan, S.A., Roberts, L.R., Cardinale, V., Carpino, G., Andersen, J.B., Braconi, C., et al. (2020). Cholangiocarcinoma 2020: the next horizon in mechanisms and management. Nat. Rev. Gastroenterol. Hepatol. *17*, 557–588. https://doi.org/10.1038/s41575-020-0310-z.

2. Feng, Q., Zhang, W., Li, Y., Yang, X., Hao, Y., Zhang, H., Li, W., Hou, L., and Zhang, Z. (2017). An intelligent NIR-responsive chelate copper-based anticancer nanoplatform for synergistic tumor targeted chemo-phototherapy. Nanoscale *9*, 15685–15695. https://doi.org/10.1039/c7nr05003h.

3. Sapisochin, G., Facciuto, M., Rubbia-Brandt, L., Marti, J., Mehta, N., Yao, F.Y., Vibert, E., Cherqui, D., Grant, D.R., Hernandez-Alejandro, R., et al. (2016). Liver transplantation for "very early" intrahepatic cholangiocarcinoma: international retrospective study supporting a prospective assessment. Hepatology *64*, 1178–1188. https://doi.org/10.1002/hep.28744.

4. Jarnagin, W.R., Fong, Y., DeMatteo, R.P., Gonen, M., Burke, E.C., Bodniewicz BS, J., Youssef BA, M., Klimstra, D., and Blumgart, L.H. (2001). Staging, resectability, and outcome in 225 patients with hilar cholangiocarcinoma. Ann. Surg. *234*, 507–517. , discussion 517-519. https://doi.org/10.1097/00000658-200110000-00010.

5. Rizvi, S., Khan, S.A., Hallemeier, C.L., Kelley, R.K., and Gores, G.J. (2018). Cholangiocarcinoma - evolving concepts and therapeutic strategies. Nat. Rev. Clin. Oncol. *15*, 95–111. https://doi.org/10.1038/nrclinonc.2017.157.

6. Rizzo, A., Ricci, A.D., and Brandi, G. (2021). Durvalumab: an investigational anti-PD-L1 antibody for the treatment of biliary tract cancer. Expert Opin. Investig. Drugs *30*, 343–350. https://doi.org/10.1080/13543784.2021.1897102.

7. Rizzo, A., and Brandi, G. (2021). First-line chemotherapy in advanced biliary tract cancer ten years after the ABC-02 trial: "and yet it moves!". Cancer Treat. Res. Commun. *27*, 100335. https://doi.org/10.1016/j.ctarc.2021.100335.

8. Sirica, A.E., and Gores, G.J. (2014). Desmoplastic stroma and cholangiocarcinoma: clinical implications and therapeutic targeting. Hepatology *59*, 2397–2402. https://doi.org/10.1002/hep.26762.

9. Robak, P., and Robak, T. (2019). Bortezomib for the treatment of hematologic malignancies: 15 Years later. Drugs R *19*, 73–92. https://doi.org/10.1007/s40268-019-0269-9.

10. Denlinger, C.S., Meropol, N.J., Li, T., Lewis, N.L., Engstrom, P.F., Weiner, L.M., Cheng, J.D., Alpaugh, R.K., Cooper, H., Wright, J.J., and Cohen, S.J. (2014). A phase II trial of the proteasome inhibitor bortezomib in patients with advanced biliary tract cancers. Clin. Colorectal Cancer *13*, 81–86. https://doi.org/10.1016/j.clcc.2013.12.005.

11. Wang, H., Cao, Q., and Dudek, A.Z. (2012). Phase II study of panobinostat and bortezomib in patients with pancreatic cancer progressing on gemcitabine-based therapy. Anticancer Res. *32*, 1027–1031.

12. Kim, G.P., Mahoney, M.R., Szydlo, D., Mok, T.S.K., Marshke, R., Holen, K., Picus, J., Boyer, M., Pitot, H.C., Rubin, J., et al. (2012). An international, multicenter phase II trial of bortezomib in patients with hepatocellular carcinoma. Invest. New Drugs *30*, 387–394. https://doi.org/10.1007/s10637-010-9532-1.

13. Li, L., Knutsdottir, H., Hui, K., Weiss, M.J., He, J., Philosophe, B., Cameron, A.M., Wolfgang, C.L., Pawlik, T.M., Ghiaur, G., et al. (2019). Human primary liver cancer organoids reveal intratumor and interpatient drug response heterogeneity. JCI Insight *4*, e121490. https://doi.org/10.1172/jci.insight.121490.

14. Alsharedi, M., and Katz, H. (2018). Check point inhibitors a new era in renal cell carcinoma treatment. Med. Oncol. *35*, 85. https://doi.org/10.1007/s12032-018-1147-y.

15. Rizvi, N.A., Mazières, J., Planchard, D., Stinchcombe, T.E., Dy, G.K., Antonia, S.J., Horn, L., Lena, H., Minenza, E., Mennecier, B., et al. (2015). Activity and safety of nivolumab, an anti-PD-1 immune checkpoint inhibitor, for patients with advanced, refractory squamous non-small-cell lung cancer (CheckMate 063): a phase 2, single-arm trial. Lancet Oncol. *16*, 257–265. https://doi.org/10.1016/S1470-2045(15)70054-9.

16. Shih, K., Arkenau, H.T., and Infante, J.R. (2014). Clinical impact of checkpoint inhibitors as novel cancer therapies. Drugs *74*, 1993–2013. https://doi.org/10.1007/s40265-014-0305-6.

17. Weber, J.S., D'Angelo, S.P., Minor, D., Hodi, F.S., Gutzmer, R., Neyns, B., Hoeller, C., Khushalani, N.I., Miller, W.H., Jr., Lao, C.D., et al. (2015). Nivolumab versus chemotherapy in patients with advanced melanoma who progressed after anti-CTLA-4 treatment (CheckMate 037): a randomised, controlled, open-label, phase 3 trial. Lancet Oncol. *16*, 375–384. https://doi.org/10.1016/S1470-2045(15)70076-8.

18. Kim, R.D., Chung, V., Alese, O.B., El-Rayes, B.F., Li, D., Al-Toubah, T.E., Schell, M.J., Zhou, J.M., Mahipal, A., Kim, B.H., and Kim, D.W. (2020). A phase 2 multi-institutional study of nivolumab for patients with advanced refractory biliary tract cancer. JAMA Oncol. *6*, 888–894. https://doi.org/10.1001/jamaoncol.2020.0930.

19. Gani, F., Nagarajan, N., Kim, Y., Zhu, Q., Luan, L., Bhaijjee, F., Anders, R.A., and Pawlik, T.M. (2016). Program death 1 immune checkpoint and tumor microenvironment: implications for patients with intrahepatic cholangiocarcinoma. Ann. Surg Oncol. *23*, 2610–2617. https://doi.org/10.1245/s10434-016-5101-y.

20. Zhou, G., Sprengers, D., Mancham, S., Erkens, R., Boor, P.P.C., van Beek, A.A., Doukas, M., Noordam, L., Campos Carrascosa, L., de Ruiter, V., et al. (2019). Reduction of immunosuppressive tumor microenvironment in cholangiocarcinoma by ex vivo targeting immune checkpoint molecules. J. Hepatol. *71*, 753–762. https://doi.org/10.1016/j.jhep.2019.05.026.

21. Bockorny, B., Semenisty, V., Macarulla, T., Borazanci, E., Wolpin, B.M., Stemmer, S.M., Golan, T., Geva, R., Borad, M.J., Pedersen, K.S., et al. (2020). BL-8040, a CXCR4 antagonist, in combination with pembrolizumab and chemotherapy for pancreatic cancer: the COMBAT trial. Nat. Med. *26*, 878–885. https://doi.org/10.1038/s41591-020-0880-x.

22. Wu, A., Maxwell, R., Xia, Y., Cardarelli, P., Oyasu, M., Belcaid, Z., Kim, E., Hung, A., Luksik, A.S., Garzon-Muvdi, T., et al. (2019). Combination anti-CXCR4 and anti-PD-1 immunotherapy provides survival benefit in glioblastoma through immune cell modulation of tumor microenvironment. J. Neuro Oncol. *143*, 241–249. https://doi.org/10.1007/s11060-019-03172-5.

23. Seo, Y.D., Jiang, X., Sullivan, K.M., Jalikis, F.G., Smythe, K.S., Abbasi, A., Vignali, M., Park, J.O., Daniel, S.K., Pollack, S.M., et al. (2019). Mobilization of CD8(+) T cells via CXCR4 blockade facilitates PD-1 checkpoint therapy in human pancreatic cancer. Clin. Cancer Res. *25*, 3934–3945. https://doi.org/10.1158/1078-0432.CCR-19-0081.

24. Tan, X.Y., Chang, S., Liu, W., and Tang, H.H. (2014). Silencing of CXCR4 inhibits tumor cell proliferation and neural invasion in human hilar cholangiocarcinoma. Gut Liver *8*, 196–204. https://doi.org/10.5009/gnl.2014.8.2.196.

25. Chen, Y., Ramjiawan, R.R., Reiberger, T., Ng, M.R., Hato, T., Huang, Y., Ochiai, H., Kitahara, S., Unan, E.C., Reddy, T.P., et al. (2015). CXCR4 inhibition in tumor microenvironment facilitates anti-programmed death receptor-1 immunotherapy in sorafenib-treated hepatocellular carcinoma in mice. Hepatology *61*, 1591–1602. https://doi.org/10.1002/hep.27665.

26. Zhao, S., Wang, J., and Qin, C. (2014). Blockade of CXCL12/CXCR4 signaling inhibits intrahepatic cholangiocarcinoma progression and metastasis via inactivation of canonical Wnt pathway. J. Exp. Clin. Cancer Res. *33*, 103. https://doi.org/10.1186/s13046-014-0103-8.

27. Li, L., Halpert, G., Lerner, M.G., Hu, H., Dimitrion, P., Weiss, M.J., He, J., Philosophe, B., Burkhart, R., Burns, W.R., et al. (2021). Protein synthesis inhibitor omacetaxine is effective against hepatocellular carcinoma. JCI Insight *6*, e138197. https://doi.org/10.1172/jci.insight.138197.

28. Høgdall, D., Lewinska, M., and Andersen, J.B. (2018). Desmoplastic tumor microenvironment and immunotherapy in cholangiocarcinoma. Trends Cancer *4*,

239–255. https://doi.org/10.1016/j.trecan.2018.01.007.

29. Massani, M., Stecca, T., Fabris, L., Caratozzolo, E., Ruffolo, C., Furlanetto, A., Morton, S., Cadamuro, M., Strazzabosco, M., and Bassi, N. (2013). Isolation and characterization of biliary epithelial and stromal cells from resected human cholangiocarcinoma: a novel in vitro model to study tumor-stroma interactions. Oncol. Rep. *30*, 1143–1148. https://doi.org/10.3892/or.2013.2568.

30. Shiga, K., Hara, M., Nagasaki, T., Sato, T., Takahashi, H., and Takeyama, H. (2015). Cancer-associated fibroblasts: their characteristics and their roles in tumor growth. Cancers *7*, 2443–2458. https://doi.org/10.3390/cancers7040902.

31. Kalluri, R., and Zeisberg, M. (2006). Fibroblasts in cancer. Nat. Rev. Cancer *6*, 392–401. https://doi.org/10.1038/nrc1877.

32. Xie, Y., Wehrkamp, C.J., Li, J., Wang, Y., Wang, Y., Mott, J.L., and Oupický, D. (2016). Delivery of miR-200c mimic with poly(amido amine) CXCR4 antagonists for combined inhibition of cholangiocarcinoma cell invasiveness. Mol. Pharm. *13*, 1073–1080. https://doi.org/10.1021/acs.molpharmaceut.5b00894.

33. Li, L., Zhang, Y., Zhou, Y., Hu, H., Hu, Y., Georgiades, C., Mao, H.Q., and Selaru, F.M. (2022). Quaternary nanoparticles enable sustained release of bortezomib for hepatocellular carcinoma. Hepatology *76*, 1660–1672. https://doi.org/10.1002/hep.32584.

34. Chen, I.X., Chauhan, V.P., Posada, J., Ng, M.R., Wu, M.W., Adstamongkonkul, P., Huang, P., Lindeman, N., Langer, R., and Jain, R.K. (2019). Blocking CXCR4 alleviates desmoplasia, increases T-lymphocyte infiltration, and improves immunotherapy in metastatic breast cancer. Proc. Natl. Acad. Sci. USA *116*, 4558–4566. https://doi.org/10.1073/pnas.1815515116.

35. Feig, C., Jones, J.O., Kraman, M., Wells, R.J.B., Deonarine, A., Chan, D.S., Connell, C.M., Roberts, E.W., Zhao, Q., Caballero, O.L., et al. (2013). Targeting CXCL12 from FAP-expressing carcinoma-associated fibroblasts synergizes with anti-PD-L1 immunotherapy in pancreatic cancer. Proc. Natl. Acad. Sci. USA *110*, 20212–20217. https://doi.org/10.1073/pnas.1320318110.

36. Rizvi, S., Fischbach, S.R., Bronk, S.F., Hirsova, P., Krishnan, A., Dhanasekaran, R., Smadbeck, J.B., Smoot, R.L., Vasmatzis, G., and Gores, G.J. (2018). YAP-associated chromosomal instability and cholangiocarcinoma in mice. Oncotarget *9*, 5892–5905. https://doi.org/10.18632/oncotarget.23638.

37. Brindley, P.J., Bachini, M., Ilyas, S.I., Khan, S.A., Loukas, A., Sirica, A.E., Teh, B.T., Wongkham, S., and Gores, G.J. (2021). Cholangiocarcinoma. Nat. Rev. Dis. Primers *7*, 65. https://doi.org/10.1038/s41572-021-00300-2.

38. Gou, M., Zhang, Y., Si, H., and Dai, G. (2019). Efficacy and safety of nivolumab for metastatic biliary tract cancer. OncoTargets Ther. *12*, 861–867. https://doi.org/10.2147/OTT.S195537.

39. van Tienderen, G.S., Li, L., Broutier, L., Saito, Y., Inacio, P., Huch, M., Selaru, F.M., van der Laan, L.J.W., and Verstegen, M.M.A. (2022). Hepatobiliary tumor organoids for personalized medicine: a multicenter view on establishment, limitations, and future directions. Cancer Cell *40*, 226–230. https://doi.org/10.1016/j.ccell.2022.02.001.

40. Diggs, L.P., Ruf, B., Ma, C., Heinrich, B., Cui, L., Zhang, Q., McVey, J.C., Wabitsch, S., Heinrich, S., Rosato, U., et al. (2021). CD40-mediated immune cell activation enhances response to anti-PD-1 in murine intrahepatic cholangiocarcinoma. J. Hepatol. *74*, 1145–1154. https://doi.org/10.1016/j.jhep.2020.11.037.

41. Loeuillard, E., Yang, J., Buckarma, E., Wang, J., Liu, Y., Conboy, C., Pavelko, K.D., Li, Y., O'Brien, D., Wang, C., et al. (2020). Targeting tumor-associated macrophages and granulocytic myeloid-derived suppressor cells augments PD-1 blockade in cholangiocarcinoma. J. Clin. Invest. *130*, 5380–5396. https://doi.org/10.1172/JCI137110.

42. Li, L., Zhang, Y., Zhou, Y., Hu, H., Hu, Y., Georgiades, C., Mao, H.Q., and Selaru, F.M. (2022). Quaternary nanoparticles enable sustained release of bortezomib for hepatocellular carcinoma. Hepatology *76*, 1660–1672.

STAR★METHODS

KEY RESOURCES TABLE

REAGENTS or RESOURCE	SOURCE	IDENTIFIER
Antibodies		
CK7 antibody	Santa Cruz	Cat#sc-23876
CK19 antibody	Abcam	Cat#ab76539
CK19 antibody	Thermofisher Scientific	Cat#10712-1-AP
Ki67 antibody	Abcam	Cat#ab15580
EPCAM antibody	Thermofisher Scientific	Cat#14-9326-82
LGR5 antibody	Abcepta	Cat#AP2745D
Collagen-1 antibody	Abcam	Cat#ab138492
α-SMA antibody	Abcam	Cat#ab150301
Ki67 antibody	BD	Cat#556003
Cleaved caspase 3 antibody	Cell Signaling Technology	Cat#9661
CD8 antibody	Thermofisher Scientific	Cat#MA1-145
CD45 antibody	Thermofisher Scientific	Cat#PA5-96061
FSP1 antibody	Abcam	Cat#ab197896
Vimentin antibody	MilliporeSigma	Cat#SAB5700782
FAP antibody	MilliporeSigma	Cat#F4771
Fc blocker anti-mouse CD16/32	BioLegend	Cat#101302
PE anti-mouse CD4	BioLegend	Cat#100511
PE-Cy7 anti-mouse CD8a	BioLegend	Cat#100721
Brilliant violet 711 anti-mouse CD45	BioLegend	Cat#103147
FITC anti-mouse CD45	BioLegend	Cat#103107
PE/cy7 anti-mouse CD11b	BioLegend	Cat#101215
Pacific blue anti-mouse Cr-1	BioLegend	Cat#108429
PE anti-mouse F4/80	BioLegend	Cat#123109
FITC anti-mouse CD3	Thermofisher Scientific	Cat#11-0032-82
Anti- mouse PD1	BioXcell	Cat#Clone RMP1-14
Chemicals, peptides and recombinant proteins		
7-ADD	BioLegend	Cat#420403
collagenase 1A	MilliporeSigma	Cat#C9891
DNase	MilliporeSigma	Cat#9003-98-9
33%/77% percoll	MilliporeSigma	Cat#P4937
Bortezomib	Selleckchem	Cat#S1013
Plerixafor	Selleckchem	Cat#S8030
RIPA lysis buffer	Cell Signaling Technology	Cat#98065
cOmplete™ Protease Inhibitor Cocktail	Roche	Cat#50-100-3301
Goat serum	Gibco	Cat#16210072
Fetal Bovine Serum	Gibco	Cat#A3840402
DMEM	Gibco	Cat#10566016
Critical commercial assays		
EPCAM positive selection kits	Stem cell technologies	Cat#17846
The proinflammatory Panel 1 mouse V-PLEX kit	Meso Scale Discovery	Cat#K15048D-1
RNeasy mini kit	Qiagen	Cat#74004

(*Continued on next page*)

Continued

REAGENTS or RESOURCE	SOURCE	IDENTIFIER
human fibrosis qRT-PCR array plate	Qiagen	Cat#330231
CellTiter-Glo® Luminescent Cell Viability Assay	Promega	Cat#G7572
SYBR Green PCR master mix	Applied Biosystems	Cat#4344463
Pierce™ BCA protein assay kit	Thermofisher Scientific	Cat#23227
Experimental models: Cell lines		
Human primary CCA PDOs	Johns Hopkins	PDO 28-5, PDO61, PDO23-3
human CCA CAFs	Johns Hopkins	CAF28-5, CAF61, CAF23-3
SB1 cell line	Mayo Clinic	Mouse SB1
Experimental models: Organisms/Strains		
Mouse C57BL/6J	The Jackson Laboratory	JAX: 000664
NOD SCID-IL2R-γ chain–deficient (NSG) mice	The Jackson Laboratory	JAX: 005557
Software and algorithms		
Flowjo-10.6	Tree Star	www.flowjo.com
GraphPad Prime 9	GraphPad software	www.graphpad.com

RESOURCE AVAILABILITY

Lead contact

Further information and requests for resources and reagents should be directed to and will be fulfilled by Dr. Florin M. Selaru (fselaru1@jhmi.edu).

Materials availability

The study did not generate new unique reagents.

Data and code availability

- Microscope data reported in this paper will be shared by the lead contact upon request. All data reported in the paper should be directed to the lead contact.
- This paper does not report original code.
- Any additional information required to reanalyze the data reported in this paper is available from the lead contact upon request.

EXPERIMENTAL MODEL AND SUBJECT DETAILS

Animal studies were approved by the Animal Care and Use Committee (ACUC) at the Johns Hopkins University. Both male and female NOD SCID-IL2R-γ chain–deficient (NSG) mice as well as C57BL/6 were purchased from Jackson Laboratory (Jackson Laboratory, Bar Harbor, ME) and housed at the animal facility of Johns Hopkins University under pathogen-free conditions. 5 to 8-week-old male and female NSG mice as well as male and female C57BL/6 mice were used for subcutaneous as well as liver orthotopic SB1 CCA cell implantation, as previously described.[36]

METHOD DETAILS

CCA patients and samples

Fresh human CCA specimens were collected at surgery at The Johns Hopkins Hospital under and informed consent approved by the Institutional Review Board.

PDO and cell line culture

CCA PDOs were established and cultured as described by us and others before.[13] Fibroblasts were isolated from the same tumors as epithelial cancer cells, identified and cultured as described.[29] Briefly, fresh human CCA tissues containing a dense stroma and fibroblasts were cut into small sizes and digested in

2.5% collagenase 1A (MilliporeSigma, Burlington, MA) and DNase for 1 to 2 h in a 37°C water bath to produce a single cell suspension. Cells were then filtered with a 100-μM strainer. A 33%/77% percoll (MilliporeSigma, Burlington, MA) was used to isolate fibroblasts from other cells within the tumor. CAFs were plated into flasks with DMEM+10% FBS and cells at passage 3–7 were used in this study, as previously described.[29] In this study, CCA PDO 28-5 and matched CAF28-5 are derived from a 56-year-old female CCA patient, 23-3 PDO and matched 23-3 CAF are derived from a 59-year-old female CCA patient, 61PDO and matched 61CAF are derived from a 45-year-old female CCA patient. SB1 mouse CCA cells were generously provided by Dr. Gregory Gores at Mayo Clinic. SB1 cells were cultured in DMEM medium supplemented with 10% FBS as described.[36] Cells are cultured in a 37 °C humidified incubator supplied with 5% CO_2.

Drug testing in complex CCA PDOs

Three CCA PDO lines and CAFs from the same patients were co-culture at a ratio of 1:1 in Matrigel for 14 days to create complex PDOs (cPDOs). BTZ, previously identified by us to be effective for epithelial CCA PDOs (ePDOs), was used in cPDOs at decreasing concentrations of 10 μM, 1 μM, 0.1 μM, 0.01 μM and 0.001 μM. Matched ePDOs cultures were treated with the same doses of BTZ. Live/dead images were captured to detect cell viability. In addition, cell TiterGlo (Promega, Madison, WI) assay was used to determine the cell viability with a plate reader (Perkin-Elmer EnVision Plate Reader, Waltham, MA). Inhibitory concentration 50 (IC50) was calculated in GraphPad Prism 9 (GraphPad Software, San Diego, CA). Co-cultured CAFs and ePDOs were separated with EPCAM positive selection kits (17846, Stem cell technologies, Vancouver, Canada).

Sustained release BTZ-loaded nanoparticle formulation

To ensure sustained treatment with BTZ without high toxicity, we have used a nanoparticle formulation of BTZ that releases BTZ over 7 days as described before,[33] The BTZ-NPs were prepared by sequentially mixing BTZ solution (1 mg/mL at DI water) with tannic acid (4 mg/mL at DI water), ovalbumin (1 mg/mL at DI water), and PEG-*b*-PLGA solution (7 mg/mL at acetonitrile) within a confined impingement jets mixer under the same method reported in our previous study.[42] The BTZ-NPs were characterized by measuring hydration radius, polydispersity index and surface charge using Zetasizer Nano ZS (Malvern Instruments, PA, USA). A transmission electron microscope (Tecnai 12 Twin, Field Electron and Ion Company, Hillsboro, OR, USA) was used to characterize morphology of nanoparticles. BTZ-NPs were suspended in 1 mL of PBS within a dialysis tube (MW 100 kDa, SpectrumLab, Waltham, MA, USA), and incubated in a 50-mL centrifuge tube containing 9 mL of PBS at 37°C on a shaker at 100 rpm to measure the release kinetics. At predetermined time points, 1% of medium outside of dialysis tube was collected and replaced with a same volume of fresh PBS. The concentration of BTZ within collected medium sample was measured with a high-performance liquid chromatography (HPLC, 1260 Infinity, Agilent Technologies, Santa Clara, CA, USA) using UV-vis spectroscopy at 280 nm with mobile phase composed of acetonitrile/water (60/40, v/v) at a flow rate of 1 mL/min. To evaluate colloidal stability, nanoparticle suspension was stored at 4 °C for 30 days; and the changes in average size and surface charge were measured during the process. After adding 9.5% trehalose as cryoprotectant, the BTZ-NPs were lyophilized at room temperature and 10 Pa using a FreeZone Traid Benchtop Freeze Dryers (Labconco, Kansas City, MO, USA). The lyophilized BTZ-NPs were stored at 4°C; and when used, the lyophilized NPs were reconstituted with the same volume of deionized water before lyophilization process. The differences in average size, surface charge and polydispersity index were measured.

Using the method described above, BTZ was successfully encapsulated within nanoparticles during a sequential flash nanocomplexation / flash nanoprecipitation process, with an average hydration radius of 72 nm. The BTZ-NPs provided a releasing duration of BTZ for 5 days, showed excellent colloidal stability. They can be reconstituted readily after lyophilization with minimal changes in average size, surface charge and polydispersity index. These BTZ-NPs can be used as an off-the-shelf formulation for efficacy study as described in this manuscript.

Animal studies

We utilized human CCA 61PDO cells (the PDOs are derived from a 45-year-old female CCA patient) to create a PDX mouse model in NSG mice. PDX tumors that reached a volume of 1 cm^3 were harvested, cut into 1 mm^3 pieces, and implanted in the right flank of additional NSG mice. Fifteen days after tumor implantation, the NSG mice were randomized into 3 groups for treatment.

An immune competent CCA mouse model was created by employing C57BL/6 male mice. In brief, SB1 cells were implanted subcutaneously in C57BL/6 mice and once the tumors grew, the animals were euthanized, tumors harvested, and cut into 1 mm^3 size to re-implanted into C57BL/6 mice. The pieces of tumor were implanted either subcutaneously or in the right liver lobe. Drug treatments were started 3 days post tumor implantation. Mice were weighted twice a week. Survival was determined in the liver implantation arm, while tumor size was measured in the subcutaneous transplantation model.

Bortezomib (Selleckchem, Houston, TX) was used to generate extended release bortezomib-nanoparticle (BTZ). BTZ was used at a dose of 1 mg/kg every 7 days. Plerixafor (Selleckchem, Houston, TX) is a CXCR4 inhibitor that was used at a concentration of 10 mg/kg/day. Anti-mouse PD1 (Clone RMP1-14, BioXcell, Lebanon, NH) or isotype control antibody (Bio X cell, Lebanon, NH) was used at a dose of 100 μg given every 3 days. All drugs were given via intraperitoneal injections.

Flow cytometry (FACS) analysis

Tumors were harvested, minced and then digested into single cell suspensions with 2.5 mg/ mL collagenase type 1 and DNase (1 mg/mL). Cell suspensions were filtered through 70 μm cell strainers, and re-suspended in cold PBS. Seven-amino-actinomycin D (7AAD, Invitrogen, Waltham, MA) was utilized to gate live cell. Cells were blocked with rat anti-mouse CD16/CD32 mAB Fc blocker for 15 min at 4°C in FACS buffer (1× PBS with 1% BSA, 0.1% sodium azide) in the dark. Surface antibody staining were then added for 1 h at 4°C in the dark, antibodies are as shown in the supplementary data. FACS data were obtained with a Sony SH800s cell sorter machine (Sony Biotechnology, San Jose CA). FACS data were analyzed using Flowjo-10.6 (Tree Star, Ashland, OR).

Gene expression analysis

RNA was extracted with Trizol and purified with RNeasy mini kit (Qiagen, Hilden, Germany). Gene expression was analyzed with a qRT-PCR array for human fibrosis (Qiagen, Hilden, Germany). We performed additional qRT-PCR reactions for other genes of interest as shown in Supplementary data. The relative gene expression was determined via real-time SYBR Green PCR master mix (Applied Biosystems, Waltham, MA) on a QuantStudio 3 machine (Applied Biosystems, Waltham, MA).

Electrochemiluminescence (ECL) assay

Frozen tumor tissues were lysed using RIPA buffer (98065, Cell Signaling) with cOmplete™ Protease Inhibitor Cocktail (Roche, Basel, Switzerland). Cell suspensions were sonicated with a sonicator (Thermofisher Scientific, Waltham, MA). The protein concentration was measured using Pierce™ BCA protein assay kit (Thermofisher Scientific, Waltham, MA). The proinflammatory Panel 1 mouse V-PLEX kit (Meso Scale Discovery, Rockville, MD) was used to measure the concentration of 3 cytokines: interferon-gamma (IFN-γ), interleukin 2 (IL-2) and tumor necrosis alpha (TNF-α) in the tumor mass.[25]

Histology and immunofluorescence (IF) staining

ePDOs and cPDOs were embedded into optimal cutting temperature (OCT) media. Frozen sections were cut with a Leica cryostat, and 10 μm slices were utilized for IF staining. Tumor specimens were fixed in 10% formalin overnight, embedded in paraffin. Sections of 6 μm were cut and stained with primary antibodies at 4°C overnight, details of antibodies are in the supplementary data then slides were incubated with Alexa fluor 488/594/647 secondary antibodies at room temperature for 1 h. DAPI was utilized for nuclear staining. Images were captured with Zeiss invert microscope or Zeiss LSM 510 confocal microscope.

QUANTIFICATION AND STATISTICAL ANALYSIS

The data were presented as mean ± standard error of the mean (SEM). GraphPad Prime 9 was used for statistical analyses. Groups were analyzed using Student's t test or by one-way ANOVA tests. Data for survival curves were analyzed with the log-rank (Mantel-Cox) test. A two-sided p-value that was smaller than 0.05 or 0.01 was considered statistically significant.